An introduction to factor analysis for radio frequency interference (RFI) detection on satellite observations

Tanvir Islam[*,1,2,3], Prashant K. Srivastava[3,4,5], Qiang Dai[3], Manika Gupta[6], Lu Zhuo[3]

[1] NOAA/NESDIS Center for Satellite Applications and Research, College Park, MD, USA

[2] Cooperative Institute for Research in the Atmosphere, Colorado State University, Fort Collins, Colorado, USA

[3] Department of Civil Engineering, University of Bristol, Bristol, UK

[4] NASA Goddard Space Flight Center, Greenbelt, MD, USA

[5] Earth System Science Interdisciplinary Center, University of Maryland, College Park, MD, USA

[6] Department of Civil Engineering, Indian Institute of Technology Delhi, New Delhi, India

***Corresponding author:**

Dr. Tanvir Islam

Center for Satellite Applications and Research (STAR)

NOAA National Environmental Satellite, Data, and Information Service

College Park, MD 20740-3818

Email: tanvir.islam@noaa.gov; tanvir.islam@msn.com

Submission

Meteorological Applications

ABSTRACT

A novel radio frequency interference (RFI) detection method is introduced for satellite-borne passive microwave radiometer observations. The method is based on factor analysis, in which, variability among observed, correlated variables are described in terms of *factors*. In this article, the method is applied to the TRMM/TMI and Aqua/AMSR-E satellite measurements over land surface to detect the RFI signals, respectively, in 10 GHz and 6 GHz channels. The RFI detection results are compared with other traditional methods, such as, spectral difference method and principal component analysis (PCA) method. It has been found that the newly proposed method is able to detect RFI signals in the C and X-band radiometer channels as effective as the conventional PCA method.

Keywords: radio-frequency interference (RFI); TRMM Microwave Imager (TMI); Advanced Microwave Scanning Radiometer - Earth Observing System (AMSR-E); passive microwave radiometry; land surface retrieval; identification algorithm;

1. INTRODUCTION

The Radio Frequency Interference (RFI) on satellite observations is known as the disturbance of electromagnetic radiation that interrupts the natural radiometric measurements by the satellite sensors. In other words, the natural thermal emission of the earth is obscured by active microwave sensors. The RFI poses a serious problem in satellite measurements, particularly at lower frequency bands, as they are mostly the un-protected bands in the microwave region (Johnson *et al.* 2006; Piepmeier *et al.* 2008; Misra *et al.* 2009; Adams *et al.* 2010). Currently, many microwave sensors are operated in unprotected bands, in order to facilitate specific geophysical retrieval. If the RFI signals are not adequately detected or removed from the satellite measurements, they can introduce significant errors in the retrieval process (Leroux *et al.* 2013). It is therefore necessary to reject the RFI signals prior to applying the retrieval algorithms on satellite measurements.

In the context of passive microwave (PMW) remote sensing, the existence of RFI errors are noted on those satellite sensors, having lower frequency channels, for instance, the SSM/I, WindSat, TMI, AMSR-E, and recently launched AMSR2 measurements. Generally speaking, the RFI locations are persistent in time and populated in urban areas (Li *et al.* 2004; Chaurasia *et al.* 2012). Therefore, a pre-processed RFI map may help to detect and remove the stationary RFI scenes, to a limited extent. Njoku *et al.* (2005) have provided a global survey of RFI contamination for 6.9 and 10.7 GHz frequencies. Nevertheless, simple RFI map is not able to detect all RFI signals, especially the signals that are not stationary and originating from new RFI sources.

As the RFI is becoming an increasingly serious hindrance in PMW remote sensing research and applications, there have recently been some progresses made to detect the RFI contamination. Primarily, many studies have found a good promise in detecting strong RFI contaminated scenes by employing simple spectral difference method (Li *et al.* 2004; Ellingson and Johnson 2006; Wu and

Weng 2011). A variation of the spectral difference method incorporating the means and standard deviations of the spectral indices has also been found effective (Njoku *et al.* 2005). Truesdale (2013) has developed a probability distribution method for computing the likelihood of brightness temperature measurements containing RFI signals. Lacava *et al.* (2013) have implemented a multi-temporal robust satellite techniques approach to identify the RFI signals. In addition, the uses of principal component analysis (PCA) indices have allowed even more accurately detecting the RFI signals (Li *et al.* 2006; Zou *et al.* 2012; Zhao *et al.* 2013).

In this paper, we propose and introduce a novel RFI detection technique that adapts the spectral difference method with factor analysis (FA) implementation. At this stage, the method is applied to the TMI and AMSR-E datasets over land surface. The method is comprehensively compared with other traditional RFI detection techniques, including, spectral difference method, PCA, and normalized PCA.

This paper is organized as follows. Section 2 provides a brief description of the datasets used. The factor analysis based RFI detection technique is introduced in Section 3. The execution of the factor analysis technique along with the results obtained from some other traditional RFI detection techniques are presented in Section 4. Section 5 offers a summary of the work.

2. DATA

The principal datasets used in this work are the TMI calibrated and AMSR-E resampled brightness temperature data.

The TMI onboard the TRMM satellite is based on the design of the Special Sensor Microwave/Imager (SSM/I). It is a multi-channel, dual polarized, conical scanning passive

microwave radiometer that measures the intensity of radiation at five separate frequencies: 10.7, 19.4, 21.3, 37, 85.5 GHz. Its swath width is 760 km on the surface. In order to maintain the consistency in measurements, two external calibration targets (one cold, one hot) are used. Spatial resolutions of the measurements vary based on the channel frequencies. Low frequency channel, that is 10.65 GHz channel, has a resolution of 63 x 37 km. By contrast, the higher-frequency channels have smaller footprint sizes (e.g. 7 x 5 km for 85.5 GHz). In depth description of the TMI instrument is described in Simpson *et al.* (1996), Islam *et al.* (2012), Islam *et al.* (2014a), and Islam *et al.* (2014b). In this article, the datasets are obtained from the Level 1B product files (1B11), available at NASA Goddard DAAC.

On the other hand, the Advanced Microwave Scanning Radiometer for EOS (AMSR-E) is a conically scanning passive microwave radiometer system that measures brightness temperatures at six frequencies starting from a C-band frequency at 6 GHz (6-89 GHz). The instrument has dual polarization capability, which leverages to separate horizontally and vertically polarized measurements at each frequency. The observations of cosmic background radiation and an on-board warm target are used to facilitate the necessary calibration of the measurements. Spatial resolution of the individual channel measurements differs from 5.4 km at 89.0 GHz to 56 km at 6.9 GHz. A comprehensive description of the AMSR-E instrument is given in Kawanishi *et al.* (2003). In this work, the brightness temperatures data are taken from AMSR-E Level-2A (AE_L2A) Global Swath Spatially-Resampled Brightness Temperatures product, obtained from NSIDC DAAC in Boulder, Colorado. That means footprint sizes for all twelve channels are spatially consistent.

3. THE RFI DETECTION METHODS

Traditionally, spectral difference method has been acknowledged as a good way to detect RFI pixels over land surface. The fundamental perception of the spectral difference method is based on the

physical phenomenon of surface emissivity with respect to frequencies. Naturally, higher frequency channels those are sensitive to land surface should have higher brightness temperature measurements than the lower frequency channels for the same polarizations:

$$TB_{Higher} - TB_{Lower} > 0 \quad (1)$$

where, TB_{Higher} and TB_{Lower} can be 6 GHz (10 GHz) and 10 GHz (18 GHz), respectively. This is mainly due to the fact that dielectric constant of water over land surface varies with respect to frequencies, and as such, the resulting surface emissivity increases with respect to frequencies. Nevertheless, if a particular frequency is contaminated by RFI signals, a reversed spectral gradient is seen as:

$$TB_{Lower} - TB_{Higher} > 0 \quad (2)$$

By using this simple spectral measurement difference (spectral index) in a given polarization, one can identify for possible RFI contamination. Previously, Yang *et al.* (2011) have mentioned that 5 K is a good threshold to detect RFI signals, based on a microwave land surface emissivity model over various land types at 10 GHz.

Due to natural radiation measured by radiometer channels, a good correlation exists between the channel measurements. Nonetheless, the spectral difference method does not account for this natural correlation between the channels in identifying RFI signals. Therefore, the spectral difference method has been incorporated with principal component analysis (PCA) by several authors, and noted as very effective for RFI detection.

Mathematically, let data matrix X to be constructed from RFI indices derived from satellite brightness temperature observations and centered so that each column has mean zero. Then, based on the singular value decomposition,

$$X = UDV^T \tag{3}$$

where, U and V are orthonormal, and D is diagonal with non-negative and decreasing values. The covariance matrix is then constructed from the data matrix X:

$$S = n^{-1}X^T X = n^{-1}VDU^T UDV^T = n^{-1}VD^2V^T \tag{4}$$

Note that PCA is based on linear combinations of X that are uncorrelated and are of high variance. On the other hand, factor analysis looks for linear combination of variables known as factors. Theoretically, the factor analysis model for $k < p$ common factors is:

$$x = \mu + \Lambda f + u \tag{5}$$

where, f is uncorrelated having unite variance, u has unknown diagonal covariance matrix Ψ, and f and u are taken to be uncorrelated.

In fact, factor analysis can be written as a model for the covariance matrix Σ of the data:

$$\mathsf{S} = \mathsf{L}\mathsf{L}^T + \mathsf{Y} \tag{6}$$

This decomposition with p x k matrix Λ introduces a k factor model. The decomposition is scale independent, therefore, this can be consdiered as a model of the correlations of the data matrix.

Since, PCA also seeks a linear space like Λf to explain the data, the covariance matrix is defined as:

$$\mathsf{S} = \mathsf{L}\mathsf{L}^T + \mathsf{X} \tag{7}$$

where, Ξ is the error matrix, which is not diagonal. Therefore,

$$\Sigma - \Psi = \Lambda\Lambda^T \tag{8}$$

where, $\Lambda = p$ x k.

Note that the data matrix *X* is comprised of RFI indices, and the RFI indices vector is prepared as a function of spectral difference signatures. For instance, for the TMI imager, a vector of five component RFI indices can be written as:

$$R_{indices} = \begin{pmatrix} TB10V - TB19V \\ TB10H - TB19H \\ TB19V - TB21V \\ TB21V - TB37V \\ TB19H - TB37H \end{pmatrix} \tag{9}$$

Besides, normalized RFI indices can be used as follows:

$$R_{indices} = \begin{pmatrix} \dfrac{TB10V - TB19V - \mu}{\sigma} \\ \dfrac{TB10H - TB19H - \mu}{\sigma} \\ \dfrac{TB19V - TB21V - \mu}{\sigma} \\ \dfrac{TB21V - TB37V - \mu}{\sigma} \\ \dfrac{TB19H - TB37H - \mu}{\sigma} \end{pmatrix} \tag{10}$$

where, μ and σ are the mean and standard deviation of the five RFI indices, respectively.

4. RESULTS AND EXECUTION

In this article, we will be investigating the RFI detection by five different techniques: spectral difference method, PCA method, normalized PCA (N-PCA) method, FA method, and normalized FA (N-Factor) method. Note that, for the normalized methods (N-PCA and N-Factor), the normalized RFI indices are used as inputs. It is also worth mentioning that scattering effects originating from snow and ice can also lower the brightness temperatures at higher frequency channels than lower frequency channels. This could result into false RFI signals. Therefore, in this work, only satellite measurements from summer period are investigated. Further, primary RFI signals are originated

from land-based sources, such as transmitters used by active commercial services. Therefore, the investigation is restricted to land surface only.

For the sake of clarity, we show the averaged spectral difference map for 10 GHz vertical polarization channel (TB10V – TB19V) for a day in Figure 1, from TRMM/TMI. It can be seen that, in some places, the brightness temperatures at low frequency channels are considerably higher than the measurements at high frequency channels (positive spectral difference). Such positive spectral difference signatures show an indication of possible RFI contamination. The difference can be as high as 10 K in some areas. The RFI contamination is more pronounced in Mexico and parts of South America, and in Western Asia.

The spectral difference signatures can further be explained through scatter plots between 10 GHz and 19 GHz channels, with the same polarization (Figure 2). The scatter plots are constructed from two different domain of interest on 1st August 2013 TMI data. The data points shown in the top panels are from the South America region, whereas, the data points given in the bottom panels are from the Western Asia region. The positive spectral differences with 5 K threshold are denoted as red and rest other points are denoted as black. Assuming 5 K as a threshold, a linear correlation exists in RFI free data points. By contrast, more than 50 K positive differences are seen at 10 GHz channel than the 19 GHz channel, implying RFI signals. Therefore, certainly, the use of spectral difference signatures as RFI indices in the PCA and FA methods would further help to detect the RFI signatures. Nevertheless, it is important to be remembered that weak RFI signals are difficult to distinguish from spectral difference signatures, due to natural geophysical variability in the measurements.

Figure 3 presents the spatial distribution of RFI detection by five different techniques. This particular example is constructed from five-day TRMM/TMI data, over the Mexico. The averaged values for the spectral difference index for vertically polarized 10 GHz band are shown. Corresponding PCA, N-PCA, Factor and N-Factor indices are also included. Higher the index score, higher the RFI contamination will be. Apparently, the RFI distributions by different methods are very similar, the figure shows. More importantly, it is encouraging to see that the newly developed RFI detection technique by the factor analysis can detect very similar to those detected by the PCA method. Such performance is evident for both factor analysis and normalized factor analysis methods.

Another example of RFI identification is shown in Figure 4 for one day averaged TMI data. The plots exhibit the RFI contaminated signals over Western part of the Asia on 1st April 2013. Again, the RFI detection by the factor analysis methods (Factor and N-Factor) is in close agreement with the PCA method (PCA and N-PCA).

Nevertheless, selecting a threshold to remove RFI signals for different techniques is quite arbitrary. Generally, a threshold of 5 as PCA index, 1 as N-PCA index, and 0.5 as Factor and N-Factor index agree well with each other in screening the RFI signals from satellite measurements. Figure 5 demonstrates the efficiency of the RFI removals by different detection techniques with the above thresholds, but for the same example, as shown in Figure 4. The thresholds used here are chosen by subjective examination. One can clearly see that factor analysis method is efficient enough to detect and screen the RFI signals. In other words, both PCA and FA methods agree reasonably well with each other in excluding the RFI signals.

Another way to examine the performance of the RFI detection is through observing the channel correlations. Naturally, microwave signals produced from different channels are highly correlated with each other. On the contrary, RFI signals are not due to natural variation of microwave radiation, rather they introduce from external targets. Therefore, in the presence of RFI signals in a given channel, the correlations of that channel to other channels will be significantly lower. As such, we construct the multi-channel correlations on RFI-contaminated and RFI-free scenes in Figure 6. This figure is constructed from multiple summer day observations separating into RFI-free and RFI-contaminated pixels, as detected by the factor analysis method. Left panel displays the correlations in RFI-free pixels and right panel displays the correlations in RFI-contaminated pixels. It can be seen that channel correlations in RFI-contaminated pixels are smaller than the RFI-free pixels.

It is worth mentioning that only one narrow band is allocated in the 10.6-10.7 GHz range to passive sensing. That is why, some RFI signals have been noted in the TMI's lowest frequency channel at 10.65 GHz (X-band). On the other hand, in the 6.7-7.1 GHz, no bandwidth is allocated to passive sensing. Therefore, more RFI contamination is expected in the AMSR-E 6.9 GHz channel (C-band). Figure 7 demonstrates the RFI signals at 6.9 GHz for vertical polarization as found by the five methods, but applied to one AMSR-E orbital pass data onboard Aqua satellite. Significant RFI signals are seen in this orbital pass. Similar to the results shown for TMI data, it is evident that the factor analysis method successfully detects the RFI signals in 6 GHz channel. One can confirm that the factor analysis method is equally effective as of the well-known PCA method. This is true for both normalized and un-normalized RFI indices.

It is important to outline that, in general, 6 GHz channel is avoided in certain geophysical retrieval algorithm (e.g. soil moisture) due to significant RFI contamination in this band. As such, with the

help of the RFI detection techniques, and by employing certain index thresholds, one can reject the possible RFI contaminated signals, prior to use the 6 GHz channel in their retrieval algorithms. This will eventually improve the geophysical retrieval, as a whole, at least on those areas, where RFI contamination is minimal.

5. CONCLUSIONS

The microwave information over land at low frequency channels is mainly used to obtain important surface properties such as soil moisture, skin temperature, and vegetation information (Gupta *et al.* 2013; Srivastava *et al.* 2013a; Srivastava *et al.* 2013b; Srivastava *et al.* 2013c). This information is extremely important for not only satellite data assimilation studies, but also for geophysical retrievals and product monitoring purpose. Furthermore, many applications are directly impacted by the geophysical products, thus satellite measurements, including the applications in hydrology, ecology, climate change, and in weather forecasting. Given the importance, it is crucial to detect and remove unwanted RFI signals from the satellite measurements.

In this communication, we present a novel RFI detection algorithm with factor analysis implementation. The method takes the advantage of channel correlations as well as the spectral differences between lower and higher frequency channels. The method is applied to X-band channels of TRMM/TMI and C-band channels of Aqua/AMSR-E satellite observations. The method is compared with some other traditional methods available in the literature, including, spectral difference method and PCA method. Similar to the traditional methods, the factor analysis method yield indices, and as such, the users can decide a subjective threshold to discard the RFI signals in the satellitetmi measurements. Based on the analysis, it is reasonable to conclude that the proposed factor analysis based RFI detection technique is an effective method at detecting the RFI signals in 6 GHz and 10 GHz channels. At the same time, due to lack of independent validation datasets, the RFI

detection models are difficult to validate. As such, the RFI detection uncertainties associated with the PCA based method itself should also to be kept in mind, while interpreting the results.

ACKNOWLEDGEMENTS

The TRMM data used in this effort were acquired as part of the NASA's Earth-Sun System Division and archived and distributed by the Goddard Earth Sciences (GES) Data and Information Services Center (DISC) Distributed Active Archive Center (DAAC). The authors also acknowledge the NASA DAAC at the National Snow and Ice Data Center for providing AMSR-E/Aqua L2A Global Swath Spatially-Resampled Brightness Temperatures-Version 3 data. The views expressed here are those of the authors solely and do not constitute a statement of policy, decision, or position on behalf of NOAA/NASA or the authors' affiliated institutions.

REFERENCES

Adams IS, Bettenhausen MH, Gaiser PW, Johnston W. 2010. Identification of Ocean-Reflected Radio-Frequency Interference Using WindSat Retrieval Chi-Square Probability. *Ieee Geoscience and Remote Sensing Letters* **7**: 406-10

Chaurasia S, Thapliyal PK, Gohil BS. 2012. Assessment of the occurrence of radio frequency interference with AMSR-E observations over India. *Advances in Space Research* **50**: 450-6

Ellingson SW, Johnson JT. 2006. A polarimetric survey of radio-frequency interference in C- and X-bands in the continental United States using WindSat radiometry. *Ieee Transactions on Geoscience and Remote Sensing* **44**: 540-8

Gupta M, Srivastava PK, Islam T, Ishak AMB. 2013. Evaluation of TRMM rainfall for soil moisture prediction in a subtropical climate. *Environmental Earth Sciences*: 1-11

Islam T, Rico-Ramirez MA, Han DW, Srivastava PK, Ishak AM. 2012. Performance evaluation of the TRMM precipitation estimation using ground-based radars from the GPM validation network. *Journal of Atmospheric and Solar-Terrestrial Physics* **77**: 194-208

Islam T, Rico-Ramirez MA, Srivastava PK, Dai Q. 2014a. Non-parametric rain/no rain screening method for satellite-borne passive microwave radiometers at 19-85 GHz channels with the Random Forests algorithm. *International Journal of Remote Sensing* **35**: 3254-67

Islam T, Srivastava PK, Rico-Ramirez MA, Dai Q, Han D, Gupta M. 2014b. An exploratory investigation of an adaptive neuro fuzzy inference system (ANFIS) for estimating hydrometeors from TRMM/TMI in synergy with TRMM/PR. *Atmospheric Research* **145**: 57-68

Johnson JT, Gasiewski AJ, Guner B, Hampson GA, Ellingson SW, Krishnamachari R, Niamsuwan N, McIntyre E, Klein M, Leuski VY. 2006. Airborne radio-frequency interference studies at C-band using a digital receiver. *Ieee Transactions on Geoscience and Remote Sensing* **44**: 1974-85

Kawanishi T, Sezai T, Ito Y, Imaoka K, Takeshima T, Ishido Y, Shibata A, Miura M, Inahata H, Spencer RW. 2003. The Advanced Microwave Scanning Radiometer for the Earth Observing System (AMSR-E), NASDA's contribution to the EOS for global energy and water cycle studies. *Ieee Transactions on Geoscience and Remote Sensing* **41**: 184-94

Lacava T, Coviello I, Faruolo M, Mazzeo G, Pergola N, Tramutoli V. 2013. A Multitemporal Investigation of AMSR-E C-Band Radio-Frequency Interference. *Ieee Transactions on Geoscience and Remote Sensing* **51**: 2007-15

Leroux DJ, Kerr YH, Richaume P, Fieuzal R. 2013. Spatial distribution and possible sources of SMOS errors at the global scale. *Remote Sensing of Environment* **133**: 240-50

Li L, Gaiser PW, Bettenhausen MH, Johnston W. 2006. WindSat radio-frequency interference signature and its identification over land and ocean. *Ieee Transactions on Geoscience and Remote Sensing* **44**: 530-9

Li L, Njoku EG, Im E, Chang PS, Germain KS. 2004. A preliminary survey of radio-frequency interference over the US in Aqua AMSR-E data. *Ieee Transactions on Geoscience and Remote Sensing* **42**: 380-90

Misra S, Mohammed PN, Guner B, Ruf CS, Piepmeier JR, Johnson JT. 2009. Microwave Radiometer Radio-Frequency Interference Detection Algorithms: A Comparative Study. *Ieee Transactions on Geoscience and Remote Sensing* **47**: 3742-54

Njoku EG, Ashcroft P, Chan TK, Li L. 2005. Global survey and statistics of radio-frequency interference in AMSR-E land observations. *Ieee Transactions on Geoscience and Remote Sensing* **43**: 938-47

Piepmeier JR, Mohammed PN, Knuble JJ. 2008. A double detector for RFI mitigation in microwave radiometers. *Ieee Transactions on Geoscience and Remote Sensing* **46**: 458-65

Simpson J, Kummerow C, Tao WK, Adler RF. 1996. On the tropical rainfall measuring mission (TRMM). *Meteorology and Atmospheric Physics* **60**: 19-36

Srivastava PK, Han DW, Ramirez MAR, Islam T. 2013a. Appraisal of SMOS soil moisture at a catchment scale in a temperate maritime climate. *Journal of Hydrology* **498**: 292-304

Srivastava PK, Han DW, Ramirez MR, Islam T. 2013b. Machine Learning Techniques for Downscaling SMOS Satellite Soil Moisture Using MODIS Land Surface Temperature for Hydrological Application. *Water Resources Management* **27**: 3127-44

Srivastava PK, Han DW, Rico-Ramirez MA, Al-Shrafany D, Islam T. 2013c. Data Fusion Techniques for Improving Soil Moisture Deficit Using SMOS Satellite and WRF-NOAH Land Surface Model. *Water Resources Management* **27**: 5069-87

Truesdale D. 2013. A Probability Distribution Method for Detecting Radio-Frequency Interference in WindSat Observations. *Ieee Transactions on Geoscience and Remote Sensing* **51**: 3780-8

Wu Y, Weng FZ. 2011. Detection and correction of AMSR-E radio-frequency interference. *Acta Meteorologica Sinica* **25**: 669-81

Yang H, Weng FZ, Lv LQ, Lu NM, Liu GF, Bai M, Qian QY, He JK, Xu HX. 2011. The FengYun-3 Microwave Radiation Imager On-Orbit Verification. *Ieee Transactions on Geoscience and Remote Sensing* **49**: 4552-60

Zhao J, Zou XL, Weng FZ. 2013. WindSat Radio-Frequency Interference Signature and Its Identification Over Greenland and Antarctic. *Ieee Transactions on Geoscience and Remote Sensing* **51**: 4830-9

Zou XL, Zhao J, Weng FZ, Qin ZK. 2012. Detection of Radio-Frequency Interference Signal Over Land From FY-3B Microwave Radiation Imager (MWRI). *Ieee Transactions on Geoscience and Remote Sensing* **50**: 4994-5003

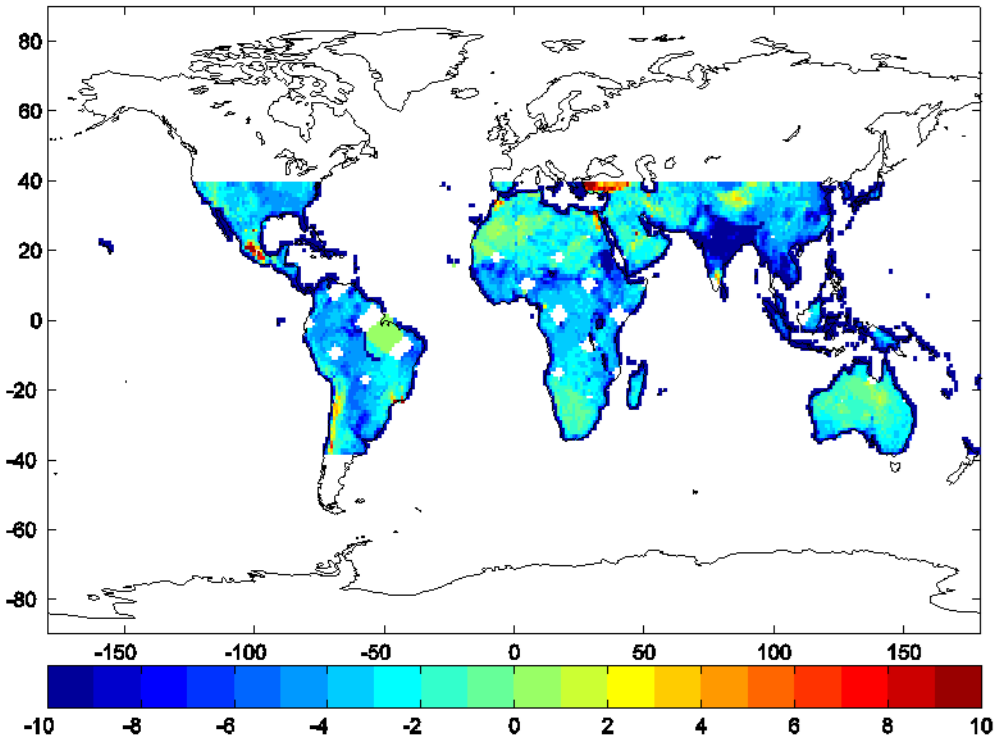

Figure 1: An example illustrating the differences in brightness temperatures between vertically polarized 10.65 and 19.35 GHz channels (TB10V – TB19V). The map is constructed from one day ascending and descending TRMM/TMI orbital samples on 1st August 2013.

.

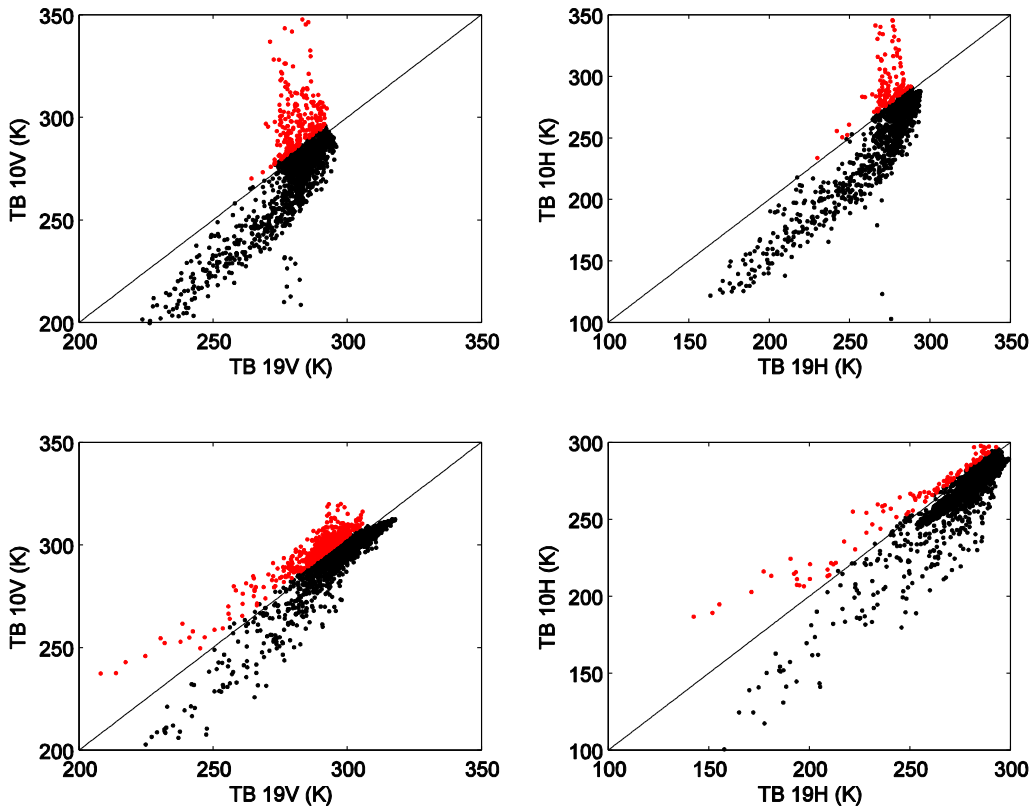

Figure 2: Scatter plots between 19 GHz and 10 GHz in vertical polarization (left) and horizontal polarization (right) channels from TRMM/TMI. Top panels are constructed from an example domain over South America and bottom panels are constructed from an example domain over X on 1st August 2013. Data points with TB10V – TB19V≥5 K are indicated in red and TB10V – TB19V<5 K are indicated in black.

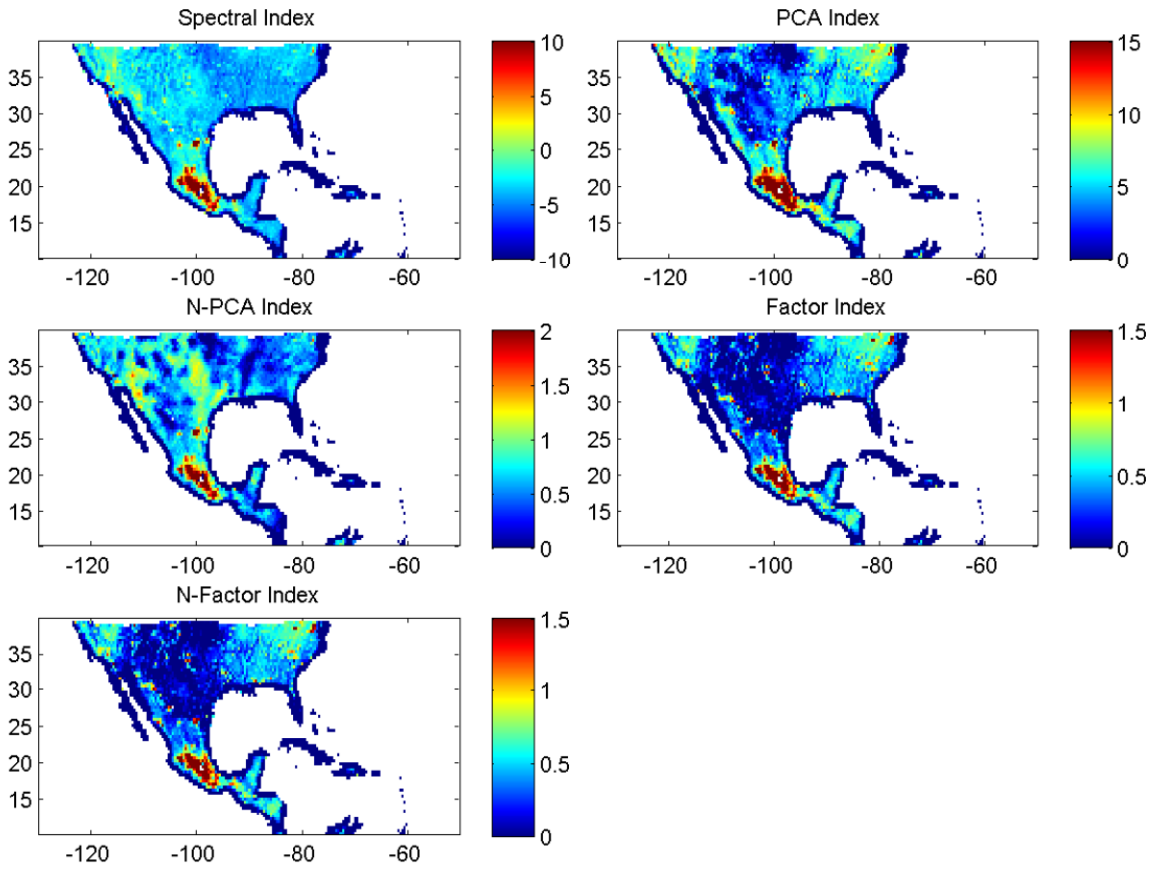

Figure 3: Spatial distribution of the RFI detection indices at 10 GHz for vertical polarization by five different RFI detection methods over South America. Data are averaged from five day TMI orbital samples.

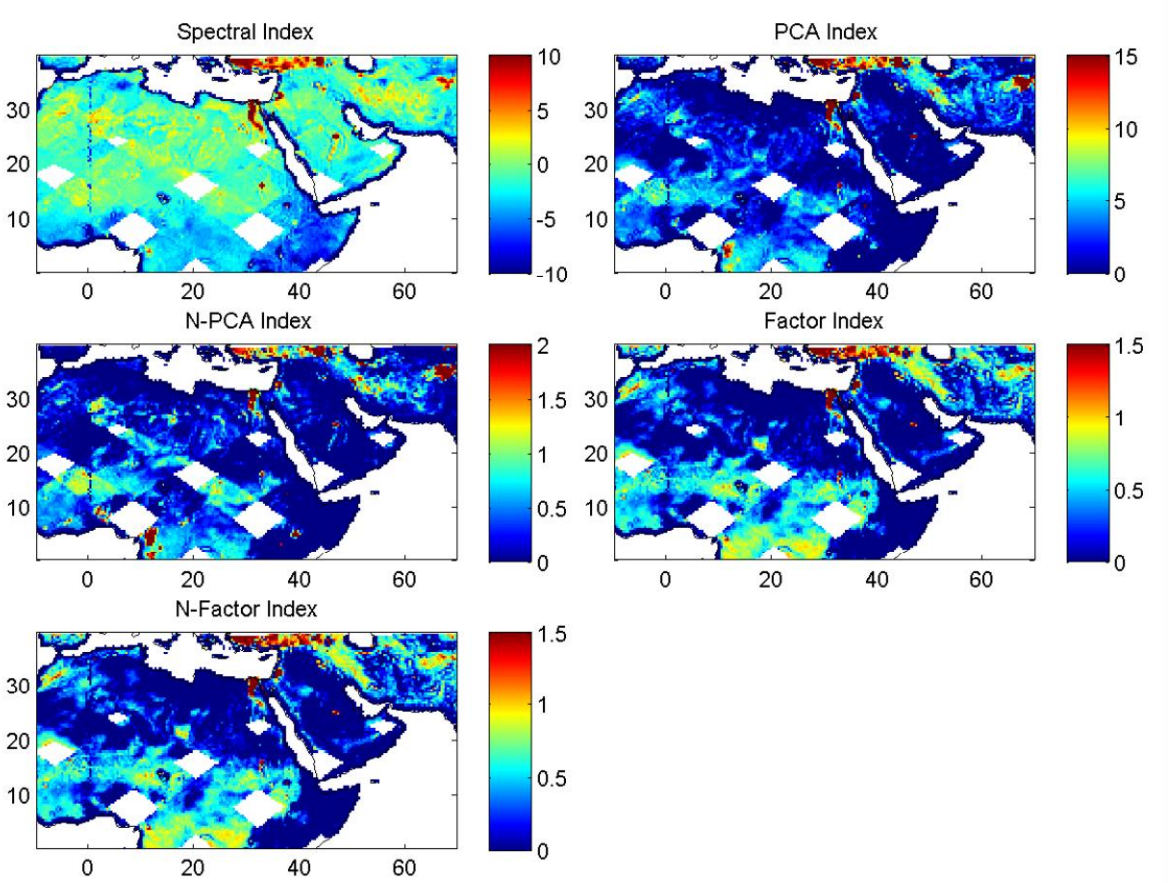

Figure 4: Spatial distribution of the RFI detection indices at 10 GHz for vertical polarization by five different RFI detection methods over Western Asia. Data are averaged from one day TMI orbital samples (1st April 2013).

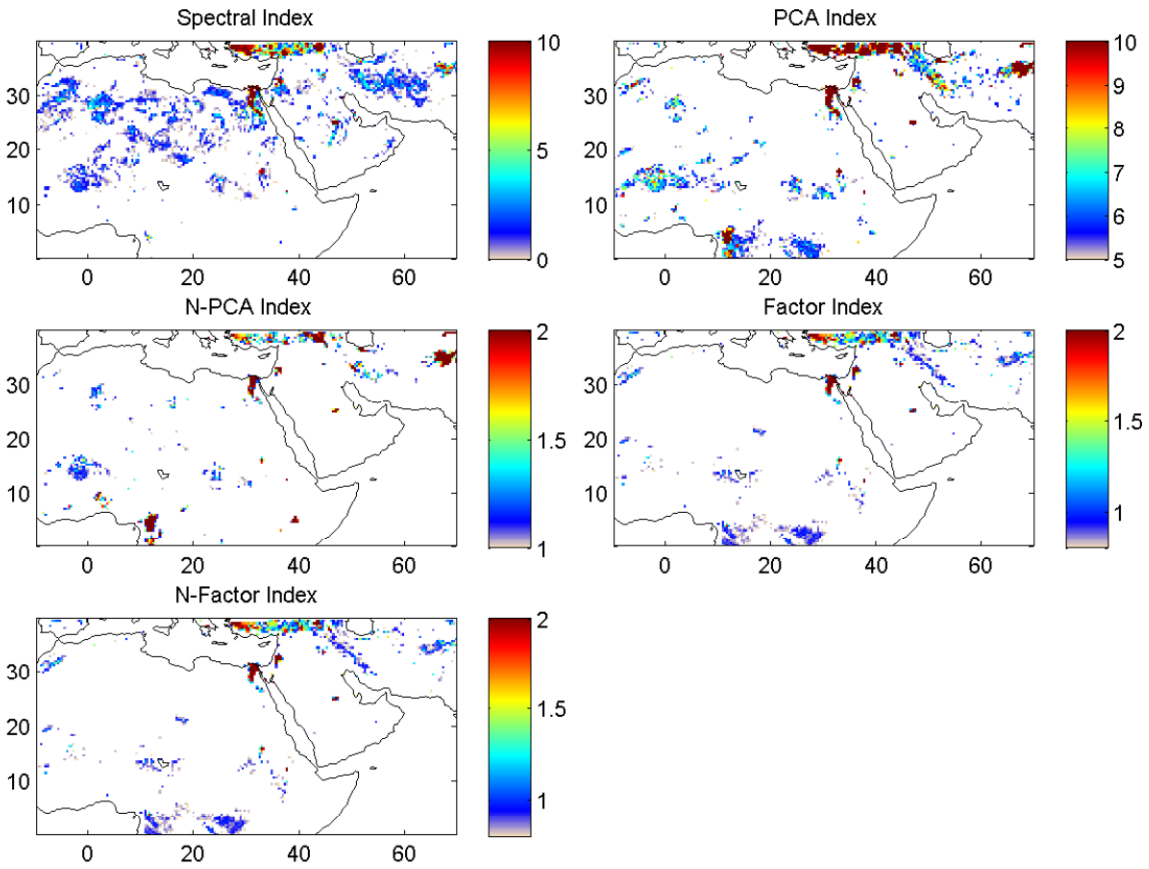

Figure 5: Same as Figure 4, but after excluding the RFI signals with applying index thresholds.

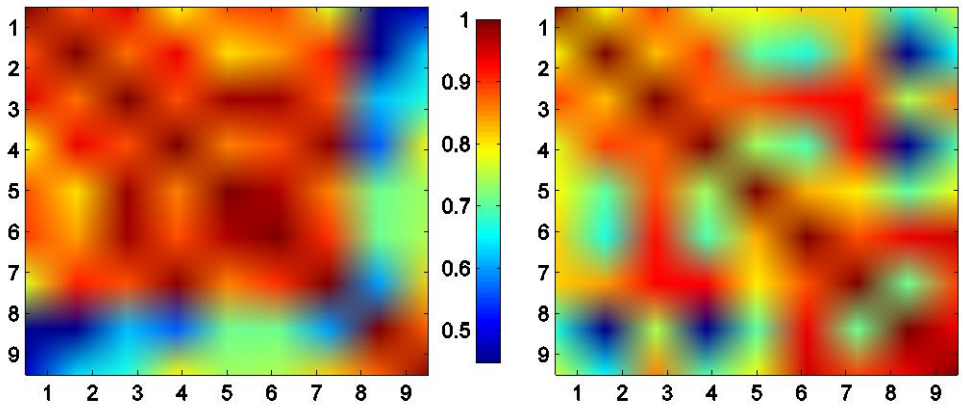

Figure 6: Correlation matrix of the TMI channels from RFI free (left) and RFI contaminated (right) scenes.

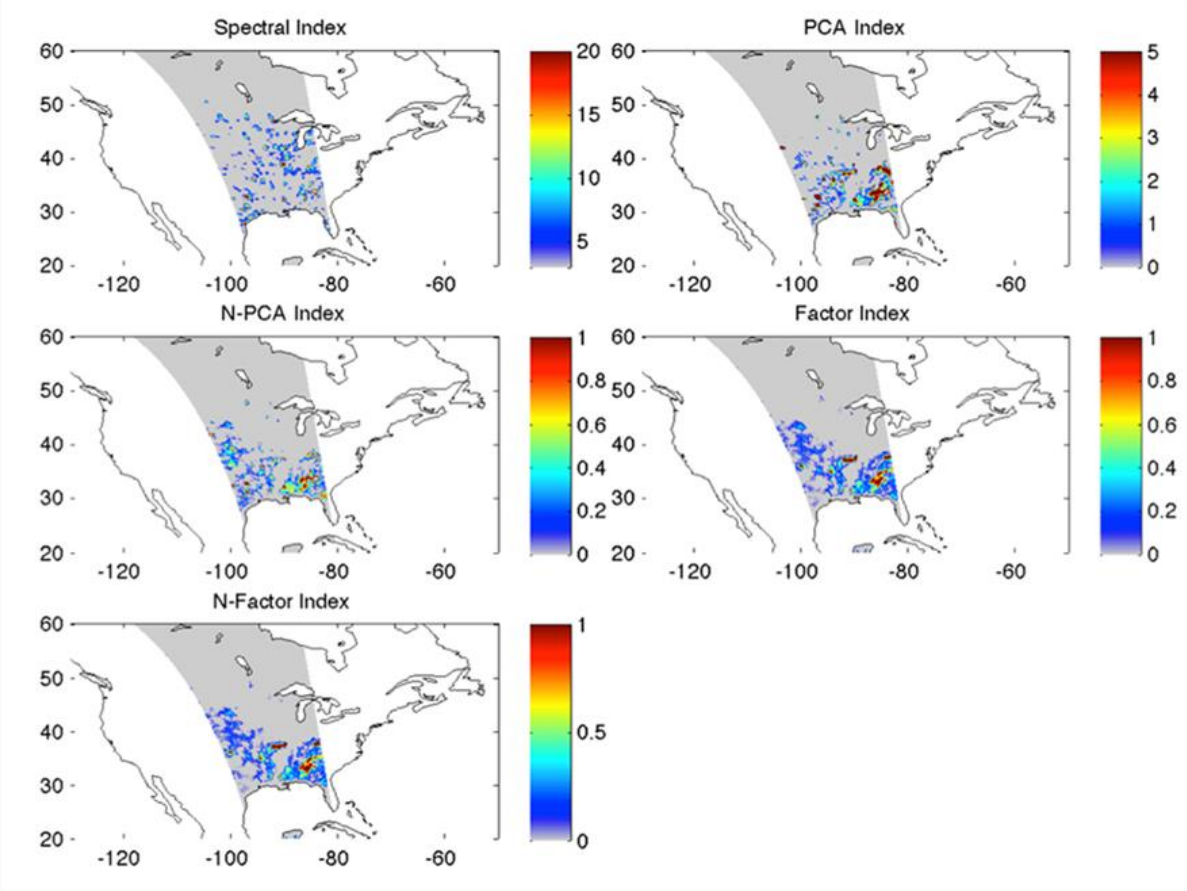

Figure 7: Spatial distribution of the RFI detection indices at 6 GHz for vertical polarization by five different RFI detection methods over Western Asia. Data are averaged from one day AMSR-E orbital samples.